Abstract of "Visualizing Fluid Flow Data:
From the Canvas to the CAVE" by Robert M. Kirby II, Sc.M., Brown University, May 2001.

Scientific visualization not only expands our understanding of fluid flow phenomena by allowing us to examine the evolution of different flow quantities, but also it can be used as a catalyst for the development of mathematical models which describe the time evolution of complex flows. We believe that the simultaneous examination of multiple flow quantities can provided a better understanding of the underlying processes of fluid flow.

This project report describes the work of three projects in which I have participated. All research contained herein had as its end goal the investigation of techniques for visualizing fluid flow data.

The first project sought to use concepts from painting for visualizing two dimensional flows. For the two dimensional flow examples, we present visualizations of three flow examples and observations concerning some of the physical relationships made apparent by the multi-valued data display technique that we employed.

The second and third projects had as a goal the use of interactive immersive environments for studying three dimensional flows. For the three dimensional flow examples, we describe the development of two components sufficient for interactive immersion in the Cave. The second project was the implementation of DOGL, an OpenGL-based library for distributed rendering systems used for distributing geometry for display on our four-wall immersive display system. The third project was the implementation of a C++ class within the Jot graphics system for visualizing fluid flow data produced by $\mathcal{NEKTAR}$. An arterial bypass flow simulation provides a case study for the combination of DOGL and $\mathcal{NEKTAR}$ simulation data for visualizing fluid flow phenomena in 3D using an interactive immersive viewing environment.

Visualizing Fluid Flow Data:
From the Canvas to the CAVE

by
Robert M. Kirby II

B.S., Applied Mathematics and Computer and Information Sciences, Florida State University, 1997
Sc.M., Applied Mathematics, Brown University, 1999

A project report submitted in partial fulfillment of the
requirements for the Degree of Master of Science
in the Department of Computer Science at Brown University

Providence, Rhode Island
May 2001

Abstract

Scientific visualization not only expands our understanding of fluid flow phenomena by allowing us to examine the evolution of different flow quantities, but also it can be used as a catalyst for the development of mathematical models which describe the time evolution of complex flows. We believe that the simultaneous examination of multiple flow quantities can provided a better understanding of the underlying processes of fluid flow.

This project report describes the work of three projects in which I have participated. All research contained herein had as its end goal the investigation of techniques for visualizing fluid flow data.

The first project sought to use concepts from painting for visualizing two dimensional flows. For the two dimensional flow examples, we present visualizations of three flow examples and observations concerning some of the physical relationships made apparent by the multi-valued data display technique that we employed.

The second and third projects had as a goal the use of interactive immersive environments for studying three dimensional flows. For the three dimensional flow examples, we describe the development of two components sufficient for interactive immersion in the Cave. The second project was the implementation of DOGL, an OpenGL-based library for distributed rendering systems used for distributing geometry for display on our four-wall immersive display system. The third project was the implementation of a C++ class within the Jot graphics system for visualizing fluid flow data produced by $\mathcal{NEKTAR}$. An arterial bypass flow simulation provides a case study for the combination of DOGL and $\mathcal{NEKTAR}$ simulation data for visualizing fluid flow phenomena in 3D using an interactive immersive viewing environment.

Acknowledgements

Acknowledgments are those things which are often written last but are presented first in the document. I am truly blessed to have had the opportunity to interact with many people in my quest for an advanced degree in Computer Science, and for this I am grateful.

First of all, I must express my gratitude to Professor George Em Karniadakis, my Ph.D. advisor in Applied Mathematics, for affording me the opportunity to work on an advanced degree in Computer Science while also working on my Ph.D. in Applied Mathematics. He has both encouraged and supported my collaboration with scientists in Computer Science and in other fields. My apprenticeship under him has refined my skills as a simulation scientist.

Secondly, I would like to thank Professor Andries van Dam, my advisor in Computer Science. From the very beginning, Andy made me feel "part of the team"; I was not considered an Applied Mathematician trying to do Computer Science, but rather I was respected and encouraged as a simulation scientist who could combine skills in both areas. Andy continually encouraged me to seek out those things which I do well, and do them better; to objectively see those areas which need improvement, and to refine them. His mentoring is very much appreciated.

Thirdly, I would like to thank Professor David Laidlaw of Computer Science. When I was starting my collaborative work with Computer Science, Andy encouraged me to work with "the new faculty member" David Laidlaw. Shortly thereafter Andy sent me to IEEE Vis'98 as part of the STC team from Brown. While at Vis, during the banquet dinner, I was able to finally meet up with David. After enjoying a nice dinner, we spoke the remainder of the evening about scientific visualization. It was during that meeting that our future collaboration, and our friendship, was birthed. I have had the opportunity to interact with David on many different levels – as a student in the classroom, as co-author on several papers, as consultant on a variety of projects, and most importantly, as a friend. His scientific insight, his humor, his candor, and most of all his friendship are greatly

appreciated.

I would like to thank those who have worked with me on the projects outlined in this report: Andy Forsberg for his assistance on a multitude of things, among them being my primary contact with the graphics group, Jon Reiter for his help with DOGL and the user-study, and Dr. Spencer Sherwin for providing me with the arterial bypass graft mesh and providing me with insight into the flow dynamics of the arterial bypass graft fluid flow simulation. I would also like to acknowledge and thank the following for their help: Sam Fulcomer, George Loriot, Loring Holden, Joe LaViola, Dr. Haralambos Marmanis, Dr. Tim Warburton and Dr. Constantinos Evangelinos.

Contents

List of Figures

Chapter 1

Introduction

The numerical simulation of fluid flow phenomena has become a scientific tool used for discovery and understanding of the principles which govern fluid flow. The data produced by numerical simulations is often processed using a variety of techniques whose purpose is to enhance our understanding of the physical phenomena. One increasingly common technique is visualization for developing physical intuition of mathematically defined quantities. Scientific visualization not only expands our understanding of fluid flow phenomena by allowing us to examine the evolution of flow quantities, but also it provides a catalyst for the development of mathematical models which describe the time evolution of complex flows.

1.1 Objective

The simultaneous display of fluid quantities can be accomplished in many ways. We have chosen to investigate two particular methods: using concepts from painting for visualizing multi-valued data for two dimensional flows, and using immersive environments for visualizing fluid flow data for three dimensional flows. The first project's focus was the visualization of two dimensional fluid flow data. The objective of the first project was to provide the *seamless* integration of multiple flow quantities into one visualization. Independent of the first project, the second and third projects focused on the visualization of three dimensional fluid flow data. Our objective was to utilize our four-walled interactive, immersive environment, referred to as a Cave [1], for fluid flow visualizations of simulation data produced by the computational fluid dynamics code $\mathcal{NEKTAR}$ [1]. A description of the particular objectives of both viewing methodologies is presented below.

[1] Here we use the term Cave to refer to our CAVE-style derivative of the original CAVE developed at the University of Illinois' Electronic Visualization Laboratory.

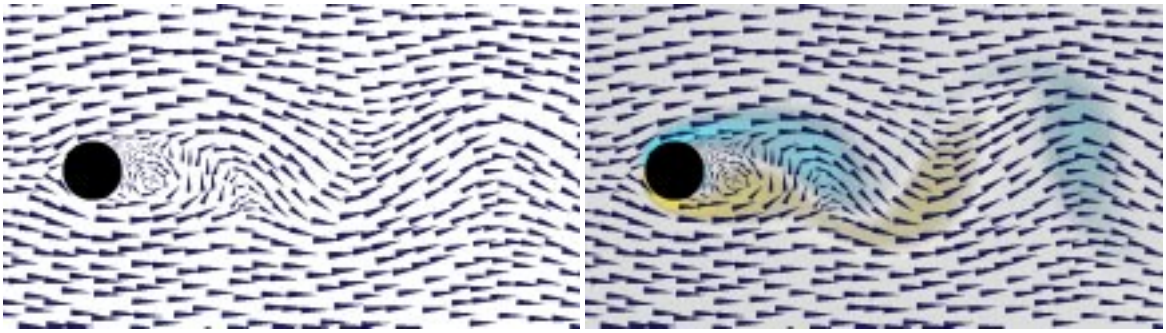

Figure 1.1: Typical visualization methods for 2D flow past a cylinder at Reynolds number 100. On the left, we show only the velocity field. On the right, we simultaneously show velocity and vorticity. Vorticity represents the rotational component of the flow. Clockwise vorticity is blue, counterclockwise yellow.

1.1.1 Visualizing Fluid Flow Using Concepts from Painting

The simultaneous examination of multiple flow quantities can provided a better understanding of the underlying processes of fluid flow. In addition to the examination of the primitive variables, i.e., the velocity and the pressure, the examination of derived quantities has provided a better understanding of the underlying processes of fluid flow.

Vorticity, a quantity denoting the rotational tendency of the fluid, is a classic example of a mathematical construct which provides information not immediately assimilated by merely viewing the velocity field. In Figure 1.1, we illustrate this idea. When examining only the velocity field, it is difficult to see that there is a rotational component of the flow in the wake region downstream of the cylinder. However when vorticity is combined with the velocity field the underlying dynamics of vortex generation and advection is more apparent.

Though vorticity cannot be measured directly, its relevance to fluid flow was recognized as early as 1858 with Helmholtz's pioneering work. Vorticity as a physical concept is not necessarily intuitive to all, yet visualizations of experiments demonstrate its usefulness, and hence account for its popularity. Vorticity is derived from velocity, and *vice versa* under certain constraints [2]. Hence, vorticity does not give any new information that was not already available from the velocity field, but it does emphasize the rotational component of the flow. The latter is clearly demonstrated in Figure 1.1, where the rotational component is not apparent when one merely views the velocity.

In the same way that vorticity as a derived quantity provides us with additional information about the flow characteristics, other derived quantities such as the rate of strain tensor, the turbulent charge and the turbulent current (all of which are defined in Chapter 3) could be of equal use. Because the examination of the rate of strain tensor, the turbulent

charge and the turbulent current within the fluids community is relatively new, few people have ever seen visualizations of these quantities in well-known fluid mechanics problems. Simultaneous display of the velocity and quantities derived from it is done both to allow the CFD researcher to examine these new quantities against the canvas of previously examined and understood quantities, and also to allow the researcher to accelerate the understanding of these new quantities by visually correlating them with well known fluid phenomena.

To demonstrate the application of these concepts, we present visualizations of a geometry that, although simple in form, demonstrates many of the major concepts which motivate our work. By examining the well studied problem of flow past a cylinder we demonstrate the usefulness of the visualizations in a context familiar to most fluids researchers. We examined two-dimensional direct numerical simulation of flow past a cylinder for Reynolds number 100 and 500 [3]. This range of Reynolds numbers provides sufficient phenomenological variation to allow us to discuss the impact of visualization of the newly visualized quantities.

We extended the visualization methods presented in [4] to problems in fluid mechanics. As in [4], we sought representations that are inspired by the brush strokes artists apply in layers to create an oil painting. We copied the idea of using a primed canvas or underpainting that shows through the layers of strokes. Rules borrowed from art guided our choice of colors, texture, visual elements, composition, and focus to represent data components. Our new methods simultaneously display 6-9 data values, qualitatively representing the underlying phenomena, emphasizing different data values to different degrees, and displaying different portions of the data from different viewing distances.

1.1.2 Visualizing Fluid Flow Using Immersive Environments

To investigate the use of interactive immersive environments for the interaction with and the visualization of three dimensional fluid flow data, we chose to study the fluid flow patterns of an arterial bypass graft. Coronary artery grafts regularly fail for unknown reasons, requiring repeated heart surgeries and often causing heart failure. Medical imaging modalities provide varying views of these arteries, via x-ray angiography, ultrasound, and magnetic resonance imaging, but simulation of the flow of blood in the vessels holds significant potential for understanding why these grafts fail. We combined the simulation capability of $\mathcal{NEKTAR}$, a CFD code for simulating fluid flow in complex three-dimensional time dependent domains with the interaction and visualization software "Jot", an in-house interactive 3D graphics system. In our attempts to use this interactive software environment in our four-wall Cave,

we had tremendous difficulty in successfully displaying on all four walls simultaneously, the primary problems being synchronization and latency issues. To this end, we developed DOGL to begin to address the distributed rendering problem at our facility where we are driving our four-wall Cave with four or more graphics adapters in multiple nodes of our IBM SP running AIX. DOGL is an acronym for "Distributed OpenGL" and describes our approach to addressing the problem: all OpenGL calls from one process are intercepted and are subsequently broadcast to multiple graphics adapters. DOGL also allows OpenGL calls to be explicitly sent to individual graphics adapters. After the development of DOGL, we were able to combine it with Jot-$\mathcal{N}\varepsilon\kappa\mathcal{T}\alpha r$ for successfully visualizing, in the Cave, the fluid flow simulation of an arterial bypass graft. In this project report we present both the design and implementation of DOGL and a discussion of the arterial bypass graft case study for which it was used.

1.2 Breakdown

In Chapter 2 we describe the painting-motivated method we employed for visualizing two dimensional fluid flow data, with specific details concerning the combination of scalar, vector, and tensor data into one visualization. We present fluid flow examples where multi-valued data visualization of two dimensional fluid flow phenomena was used. In Chapter 3 we present a description of the design and implementation of DOGL, the distributed OpenGL software used to allow Jot to display in our four-wall interactive immersive viewing environment. In Chapter 4 we present a case study of combining $\mathcal{N}\varepsilon\kappa\mathcal{T}\alpha r$, Jot and DOGL for the immersive viewing of and interaction with an arterial bypass graph fluids simulation. We briefly describe the biological problem, the numerical simulation methodology, and the immersive virtual Cave environment. In Chapter 5 we conclude by summarizing the contributions of this project report, with specific emphasis to which components of this multi-person work were specifically mine, along with presenting the lessons learned from these endeavors.

Chapter 2

Visualizing Fluid Flow with Concepts from Painting

Artists have the ability to take a tremendous amount of information and compose it into a painting. Even the simplest of paintings can consist of many pieces of information, all interconnected and intertwined in such a way that it presents a cohesive whole. Scientific visualization can be viewed as the simultaneous display of many quantities, which the objective being to display the information in such a way that the inherent structure and interconnection between the different quantities is apparent. We desired to extend concepts from painting to fluid flow visualization.

2.1 Related Work

2.1.1 Multi-valued Data Visualization

Hesselink et al. [5] give an overview of research issues in visualization of vector and tensor fields. While they describe several methods that apply to specific problems, primarily for vector fields, the underlying data are still difficult to comprehend; this is particularly true for tensor fields. The authors suggest that "feature-based" methods, i.e., those that visually represent only important data values, are the most promising research areas, and our approach embraces this idea.

Statistical methods such as principal component analysis (PCA) [6] and eigenimage filtering [7] can be used to reduce the number of relevant values in multi-valued data. In reducing the dimensionality, these methods inevitably lose information from the data. Our approach complements these data-reduction methods by increasing the number of data

values that can be visually represented.

Different visual attributes of icons can be used to represent each value of a multi-valued dataset. In [8], temperature, pressure, and velocity of injected plastic are mapped to geometric prisms that sparsely cover the volume of a mold. Similarly, in [9] data values were mapped to icons of faces: features like the curve of the mouth or size of the eyes encoded different values. In both cases, the icons capture many values simultaneously but can obscure the continuous nature of fields. A more continuous representation using small line segment-based icons shows multiple values more continuously [10]. Our work builds upon these earlier types of iconic visual representation.

Layering has been used in scientific visualization to show multiple items: in [11, 12], transparent stroked textures show surfaces without completely obscuring what is behind them. These results are related to ours, but our application is 2D, and so our layering is not as spatial as in the 3D case. Our layering is more in the spirit of oil painting where layers are used more broadly, often as an organizing principle.

2.1.2 Flow Visualization

A number of flow-visualization methods display multi-valued data. The examples in [13, 14] combine surface geometries representing cloudiness with volume rendering of arrows representing wind velocity. In some cases, renderings are also placed on top of an image of the ground. Unlike our 2D examples, however, the phenomena are 3D and the layering represents this third spatial dimension. Similarly, in [15], surface particles, or small facets, are used to visualize 3D flow: the particles are spatially isolated and are again rendered as 3D objects.

A "probe" or parameterized icon can display detailed information for one location within a 3D flow [16]; it faithfully captures velocity and its derivatives at that location, but does not display them globally. Our data contain fewer values at each location, because we are working with 2D flow, but our visualization methods display results globally instead of at isolated points.

Spot noise [17] and line integral convolution [18] methods generate texture with structure derived from 2D flow data; the textures show the velocity data but do not directly represent any additional information, e.g., divergence or shear. The authors of [17] mention that spot noise can be described as a weighted superposition of many "brush strokes," but they do not explore the concept. Our method takes the placement of the strokes to a more carefully structured level. Of course, placement can be optimized in a more sophisticated manner,

as demonstrated in [19]; we would like to explore combining these concepts with ours. Currently our stroke placement is simple and quick to implement while providing adequate results.

2.1.3 Computer Graphics Painting

Reference [20] was the first to experiment with painterly effects in computer graphics. Reference [21] extended the approach for animation and further refined the use of layers and brush strokes characteristic for creating effective imagery. Both of these efforts were aimed toward creating art, however, and not toward scientific visualization. Along similar lines, references [22, 23, 24] used software to create pen and ink illustrations for artistic purposes. The pen and ink approach has successfully been applied to 2D tensor visualization in [25].

In reference [4], painterly concepts as used in our work were presented for visualizing diffusion tensor images of the mouse spinal cord. In that work both a motivation and a methodology for the techniques used here were presented. The goal of our work was to visualize simultaneously both new and commonly used scientific quantities within the field of fluid mechanics by building on those concepts.

2.2 Visualization methodology

The work described here was presented at IEEE Visualization '99 in [26]. This work was build upon the methodology and system of [4]. We review the methodology here. Developing a visualization method involves breaking the data into components, exploring the relationships among them, and visually expressing both the components and their relationships. For each example we explored different ways of breaking down the data so that we could gain understanding as to how the components were related. Once we achieved an initial understanding, we proceeded to the next step: designing a visual representation.

In the design, we used artistic considerations to guide how we mapped data components to visual cues of strokes and layers. Our brush strokes are affinely transformed images with a superimposed texture. In choosing mappings we looked for geometric components and mapped them to geometric cues like the length or direction of a stroke. We considered the relative significance of different components and mapped them to cues that emphasized them appropriately. For example, two related parameters could map to the length and width of a stroke, giving a clear indication of their relative values. We also considered the order in which components would best be understood and mapped earlier ones to cues that

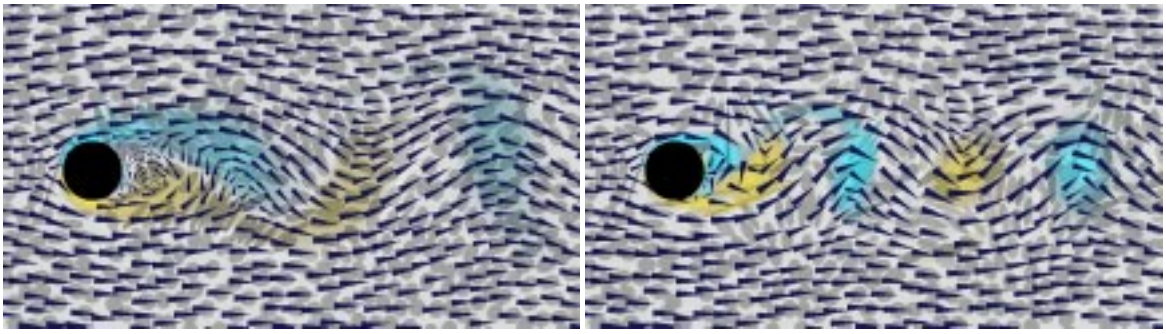

Reynolds number 100 simulated flow Reynolds number 500

data	**visualization**
velocity	arrow direction
speed	arrow area
vorticity	underpainting/ellipse color (blue=cw, yellow=ccw), and ellipse texture contrast
rate of strain	log(ellipse radii)
divergence	ellipse area
shear	ellipse eccentricity

KEY

Figure 2.1: Visualization of simulated 2D flow past a cylinder at Reynolds number = 100 and 500 (top left and top right) Velocity, vorticity, and rate of strain (including divergence and shear) are all encoded in the layers of this image. With all six values at each point visible, the image shows relationships among the values that can verify known properties of a particular flow or suggest new relationships between derived quantities.

would be seen more quickly. The set of mappings we selected defined a series of stroke images and a scheme for how to layer them.

An iterative process of analysis and refinement followed. Sometimes our refinements involved choosing a mapping we found effective in one visualization and incorporating it into another. Sometimes we needed to change the emphasis among data components by adjusting transparency, size, or color or by representing a component with a different or additional mapping. Sometimes we needed to go further back in the process and choose a new way of breaking down the data.

2.3 Example 1: Rate of strain tensor

The rate of strain tensor (sometimes called the deformation-rate tensor [27]), is a commonly used derived quantity within fluid mechanics. Though commonly used and reasonably well comprehended, few have visualized this tensor due to the added complexity necessary to view multi-valued data. Our motivation for combining visualization of the rate of strain tensor with velocity and vorticity was that despite many years of intense scrutiny, scientific understanding of fluid behavior is still not complete, and qualitative descriptions can still be helpful. Researchers often examine images of individual velocity-related quantities. We thought that good intuition might come from a visual representation that related these values to one another in a single image.

2.3.1 Data breakdown

We began by choosing a breakdown of data values into components that can be mapped onto stroke attributes. Both the velocity and its first spatial derivatives have meaningful physical interpretations [27], and hence we treat them independently. The velocity is a 2-vector with a direction and a magnitude in the plane, and can be visually mapped directly. The spatial derivatives of velocity form a second-order tensor known at the velocity gradient tensor. This tensor can be written as the sum of symmetric and antisymmetric parts,

$$\frac{\partial u_i}{\partial x_j} = \frac{1}{2}\left(\frac{\partial u_i}{\partial x_j} + \frac{\partial u_j}{\partial x_i}\right) + \frac{1}{2}\left(\frac{\partial u_i}{\partial x_j} - \frac{\partial u_j}{\partial x_i}\right), \tag{2.1}$$

$$= e_{ij} + \Omega_{ij}. \tag{2.2}$$

The antisymmetric part Ω_{ij} reduces to the vector quantity vorticity ($\omega_k = \frac{1}{2}\epsilon_{ijk}\Omega_{ij}$), and the symmetric part e_{ij} is known as the rate of strain tensor [28]. The vorticity field determines the axis and the magnitude of rotation for all fluid elements. The rate of strain tensor determines the rate at which a fluid element changes its shape under the particular flow conditions. In incompressible flows, the instantaneous rate of strain consists always of a uniform elongation process in one direction and a uniform foreshortening process in a direction perpendicular to the first. That is, a small circle will change its shape into an ellipse, whose major and minor axes represent the rate of elongation and the rate of squeezing, respectively. In compressible flows, the latter statement is not necessarily true since expansion and compression is allowed. Nevertheless, the visualization of the rate of strain remains valuable and instructive in these flows as well.

2.3.2 Visualization design

We wanted the viewer to first read velocity from the visualization, then vorticity and its relationship to velocity. Because of the complexity of the second-order rate of strain tensor we want it to be read last. We describe the layers here from bottom up, beginning with a primed canvas, adding an underpainting, representing the tensor values transparently over that, and finishing with a very dark, high-contrast representation of the velocity vectors.

• **Primer** The bottom layer of the visualization is light gray, selected because it would show through the transparent layers to be placed on top.

• **Underpainting** The next layer encodes the scalar vorticity value in semi-transparent color. Since the vorticity is an important part of fluid behavior, we emphasized it by mapping it onto three visual cues: color, ellipse opacity, and ellipse texture contrast (see below). Clockwise vorticity is blue and counter-clockwise vorticity yellow. The layer is almost transparent where the vorticity is zero, but reaches 75% opacity for the largest magnitudes, emphasizing regions where the vorticity is non-zero.

• **Ellipse layer** This layer shows the rate of strain tensor and also gives additional emphasis to the vorticity. The logarithms of the rates of strain in each direction scale the radii of a circular brush shape to match the shape that a small circular region would have after being deformed. The principal deformation direction was mapped to the direction of the stroke to orient the ellipse. The strokes are placed to cover the image densely, but with minimal overlap. The color and transparency of the ellipses are taken from the underpainting, so they blend well and are visible primarily where the vorticity magnitude is large. Finally, a texture whose contrast is weighted by the vorticity magnitude gives the ellipses a visual impression of spinning where the vorticity is larger.

• **Arrow layer** The arrow layer represents the velocity field measurements: the direction of the arrows is the direction of the velocity, and the brush area is proportional to the speed. We chose a dark blue to contrast with the light underpainting and ellipses, to make the velocities be read first. The arrows are spaced so that strokes overlap end-to-end but are well separated side-to-side. This draws the eye along the flow.

• **Mask layer** The final layer is a black mask covering the image where the cylinder was located.

These painting concepts help create a visual representation for the data that encodes all of the data in a manner that allows us to explore the data for a more holistic understanding.

2.3.3 Observations

Figure 2.1 (top left and top right) shows visualizations of 2d flow simulation results obtained using Hybrid $\mathcal{N}\varepsilon\kappa\mathcal{T}\alpha r$ [1], a spectral element code for solving the incompressible Navier-Stokes equations. These results were obtained from the work presented in [3].

The visualization of single quantities is useful by itself. For instance, if we contrast the simulation results (Figure 2.1 top right and left) with the experimental data of the airfoil (Figure 2.1 bottom), we observe that all the ellipses have the same area in the former case whereas they do not have the same area in the latter case. In incompressible flows, the continuity equation implies that the velocity field is divergence-free, which in turn implies that the trace of the rate of strain tensor (i.e. the sum of its diagonal elements) is always zero. This simply means that the area of the fluid elements remains constant in time, regardless of their instantaneous shape. Hence, we can infer that the simulation has reproduced properly the incompressible character of the fluid flow whereas the airfoil data show either compressibility effects or out of plane motion, neither of which can easily be detected by other means.

The multi-valued data visualization, however, has additional merits. For instance, we observe that the simultaneous viewing of the vorticity field and the rate of strain tensor provides us with a physical understanding about the deformation of the fluid elements. It clearly shows that at the centers of the vortices the deformation can be rather small, dependent on the eccentricity of the fluid element with respect to the center of the vortex, whereas at the edges of vortices the fluid elements suffer a huge shearing effect. Thus the mathematical decomposition of the velocity gradient tensor (i.e. $\partial u_i/\partial x_j$) into its symmetric (i.e. the rate of strain) and antisymmetric (i.e. the vorticity) parts acquires a visual representation.

Until now the deformation of the fluid elements was represented with qualitative sketches [29] whose direct connection to the rest of the flow field was not obvious. Through our visualization technique, we obtain not only the qualitative character of the fluid element deformation but also its quantitative properties. Moreover, all the information about the deformation can now be visually correlated to the velocity and the vorticity fields.

2.4 Example 2: Turbulent charge and turbulent current

Turbulent charge and turbulent current are flow quantities that have not been extensively visualized. Our motivation for viewing these quantities, in conjunction with other well-studied quantities (e.g. the vorticity), has its roots in our desire to solve problems that are concerned with *drag reduction*. The importance of fluid mechanics to the problem of reducing the drag on a moving body is unequivocal. All airplane, boat, and car designers, at some stage of their research, have consulted engineers about possible ways of reducing the drag. This is quite reasonable, since drag reduction translates to less fuel consumption.

One method of reducing the drag on a body is the appendage of riblets on the surface of the body. Though experimentally verified, the physical mechanism behind the drag reduction is not well understood. For example, some configurations and shapes of riblets do give drag reduction but some others do not. Thus, the question arises as to why this happens. What are the shapes and which are the configurations that produce drag reduction? The use of riblets everywhere on the surface is costly, thus another question is: what is the location, on the surface of an object, that will provide maximum drag reduction? The answers to the above questions can be found by inspecting visually the turbulent charge on the surface of the body [30].

Suppose we are interested in reducing the drag on a submarine. Our goal from the engineering standpoint is to find geometric modifications to our structure so that we get reasonable drag reduction with a minimum cost (and without inhibiting the purpose of our submarine). Modeling the turbulent charge on the surface of the submarine immediately delineates those regions of the geometry which could most benefit from drag reduction techniques. Unlike all other drag reduction models, the concept of turbulent charge and turbulent current succinctly provide information that is applicable to engineering design.

Unlike the case of simple flows, which can be described easily in terms of vorticity, there are cases in which the visualization of vorticity, and the subsequent description of the flow by it, can be as complex as the one in terms of velocity. For example, in the case of turbulent flows, vortices are shed from the boundaries of the flow domain, they are convected away from it, and subsequently interact with each other in a fashion that has defied a satisfactory solution of practical importance for more than a century. Hence, we can legitimately ask whether we can find other quantities whose visualization in these cases can be as beneficial to our understanding as vorticity is in more simple flows.

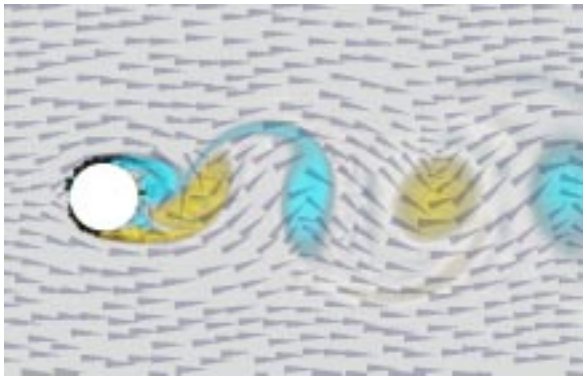

KEY	
data	**visualization**
velocity	arrow direction
speed	arrow area
vorticity	underpainting: blue=cw, yellow=ccw
turbulent charge	stroke color
turbulent current	stroke direction/area

Figure 2.2: Visualization of the turbulent charge and the turbulent current for a Reynolds number 500 simulated flow. Observe that charge concentrates near the cylinder and is negligible in other parts the flow. The cylinder geometry is now white to contrast with the visual representation for the turbulent sources

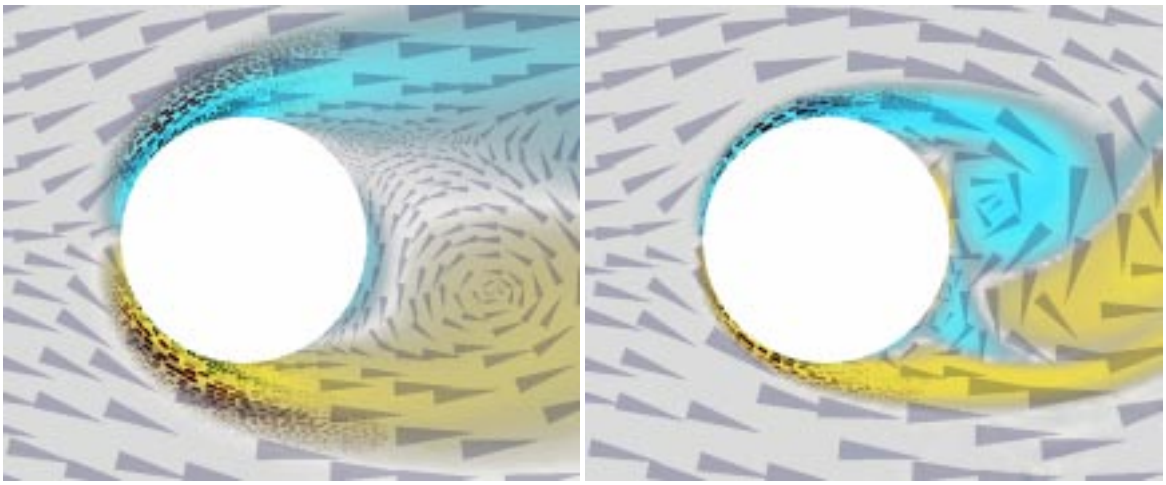

Reynolds number 100 Reynolds number 500

Figure 2.3: Close up visualization of the turbulent charge and the turbulent current at Reynolds number 100 and 500 (left and right). We are able to see the high concentrations of negative charge at the places where vorticity is being generated.

2.4.1 Data breakdown

We began by choosing a breakdown of data values into components that can be mapped onto stroke attributes. It has recently been suggested that two newly introduced quantities, namely, the turbulent charge $n(\mathbf{x}, t)$ and the turbulent current $\mathbf{j}(\mathbf{x}, t)$, collectively referred to as the turbulent sources, could substitute the role of vorticity in more complicated flows.

The nomenclature is not coincidental, it reflects the fact that the derivation of these quantities was based on an analogy between the equations of hydrodynamics and the Maxwell equations [31].

In particular, if we denote by $\mathbf{u}$ the velocity and by p the pressure then the vorticity, $\mathbf{w}$, is given by $\nabla \times \mathbf{u}$, and the Lamb vector is given by $\mathbf{l} \equiv \mathbf{w} \times \mathbf{u}$. The turbulent sources are given by the following expressions:

$$n(\mathbf{x}, t) \equiv \nabla \cdot \mathbf{l}(\mathbf{x}, t) = -\nabla^2 \left(\frac{p}{\rho} + \frac{u^2}{2} \right) , \tag{2.3}$$

and

$$\mathbf{j} = \mathbf{u}n + \nabla \times (\mathbf{u} \cdot \mathbf{w})\mathbf{u} + \mathbf{w} \times \nabla \left(\frac{p}{\rho} + \frac{3u^2}{2} \right) + 2(\mathbf{l} \cdot \nabla)\mathbf{u} . \tag{2.4}$$

The later two quantities (i.e. n, $\mathbf{j}$) are related to each other through a continuity type of equation where the turbulent current is the flux of the turbulent charge. In the cases where turbulent charge is generated solely at the wall, small turbulent charge implies small turbulent current.

2.4.2 Visualization design

We designed the turbulent source visualizations so that the overall location of the turbulent charge would be visible early. The vorticity was our next priority, since comparison between the two quantities was important. Our third priority was the structure of the flow, as represented by the velocity field. Finally, we wanted fine details about the structure of all the fields, charge, current, velocity, and vorticity, available upon close examination.

We describe the layers here from bottom up, as in the last example. Beginning with the same primed canvas and underpainting, continuing with a low-contrast representation of the velocity vectors, and finishing with a high-contrast representation of the turbulent sources. A final layer represents the geometry of the cylinder.

- **Primer and underpainting** Same as first example.

- **Arrow layer** The arrow layer for this example has the same geometric components – brush area proportional to speed, velocity direction mapped to brush direction, and strokes arranged closer end-to-end to give a sense of flow. This layer differs in that its emphasis is decreased. It has a low contrast with the layers below it. The low contrast is partly achieved through the choice of a light color for the arrows and partly through transparency of the arrows. Without the transparency, the arrows would appear very independent of the underlying layers.

• **Turbulent sources layer** In this layer we encode both the turbulent charge and the turbulent current. The current, a vector, is encoded in the size and orientation of the vector value just as the velocity in the arrow layer. The scalar charge is mapped to the color of the strokes. Green strokes represent negative charge and red strokes positive. The magnitude of the charge is mapped to opacity. Where the charge is large, we get dark, opaque, high-contrast strokes that strongly emphasize their presence. Where the charge is small, the strokes disappear and do not clutter the image. For these quantities, that tend to lie near surfaces, this representation makes very efficient use of visual bandwidth. The strokes in this layer are much smaller than the the strokes in the arrow layer. This allows for finer detail to be represented for the turbulent sources, which tend to be more localized. It also helps the turbulent sources layer to be more easily distinguished from the arrows layer than in the previous visualization, where the stroke sizes were closer and, therefore, harder to disambiguate visually.

• **Mask layer** The final layer is a mask representing the geometry of the cylinder. The mask is white in this example to contrast better with the turbulent sources layer.

2.4.3 Observations

The regions where the turbulent charge achieves its maximum values are the regions where the vorticity field has also very large values. Nevertheless, as we have already mentioned, the advantage in thinking of terms of turbulent charge is related to its permanence close to the boundaries, in contrast to the vorticity field which is conveyed downstream.

The theory proposed in [31] predicts that the turbulent charge, n, and turbulent current, $\mathbf{j}$, are the source terms (those terms for which no evolution equation is given and hence need to be inputed as part of the definition of the problem) of the following linear system of equations

$$\begin{aligned} \nabla \cdot \mathbf{W} &= 0\,, \\ \frac{\partial \mathbf{W}}{\partial t} &= -\nabla \times \mathbf{L} - \nu \nabla \times \nabla \times \mathbf{W}\,, \\ \nabla \cdot \mathbf{L} &= N(\mathbf{x}, t)\,, \\ \frac{\partial \mathbf{L}}{\partial t} &= c^2 \nabla \times \mathbf{W} - \mathbf{J}(\mathbf{x}, t) + \nu \nabla \times \nabla \times \mathbf{L}\,, \end{aligned} \tag{2.5}$$

where $c^2 = \langle u^2 \rangle$, and the use of capital letters denotes that the corresponding quantities have been spatially filtered. From these equations it can be shown that the turbulent current is the dominant forcing term for the velocity. An immediate consequence of this is that the turbulent current and the velocity field should be aligned. In Figure 2.3 we observe this

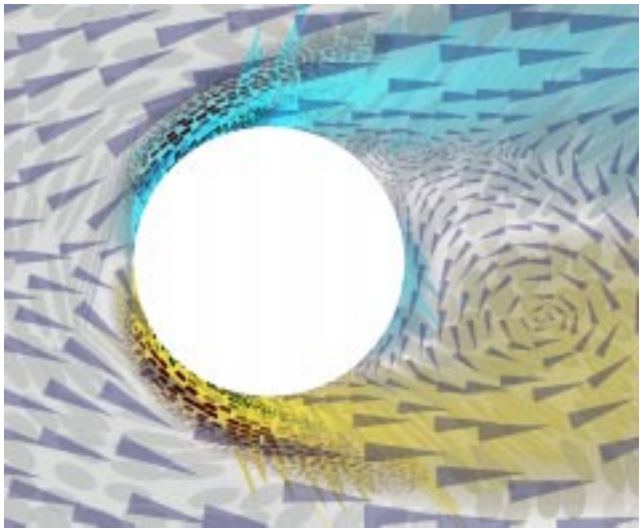

Figure 2.4: Combination of velocity, vorticity, rate of strain, turbulent charge and turbulent current for Reynolds number 100 flow. A total of nine values are simultaneously displayed.

alignment, especially in the region near the cylinder where we have the most significant change of flow velocity.

Finally, in Figure 2.4, we add the rate of strain tensor to the turbulent sources visualization, adjusting the blending of the different layers to control their relative emphasis. We observe that the high values of turbulent charge are associated with an extreme deformation of the fluid elements, since it is the shear between adjacent fluid layers that transforms the kinetic energy of the fluid to molecular heat.

Visualizing the turbulent sources is very informative for turbulent non-equilibrium flows. In fact, a plot of the turbulent charge distribution immediately allows us to determine whether a particular configuration of the riblets, discussed earlier, is reducing or enhancing the drag. A plot of the turbulent current can immediately reveal which flow directions are dominant (e.g. the streamwise direction in a pipe flow), even if no other information about the flow field is given. The distribution of the turbulent sources reflects succinctly the responses of the flow due to boundary conditions or external fields.

2.5 Preliminary User-Study Results

To test the effectiveness of painterly methods for visualizing fluid flow quantities, a pilot user-study was initiated by Jon Reiter, Joe LaViola, David Laidlaw and myself. The purpose

of this study was to compare traditional visualization methods with the painterly methods discussed in this thesis. Eight Brown University students were asked a series of questions on sample visualizations produced by traditional and painterly methods. We found that subjects were 13% more accurate for determining where a scalar field's value was greater in the artistic images over traditional ones. Subjects were 4% more accurate for vector magnitude comparisons when using the artistic methods, and subjects were 18% more accurate when asked questions pertaining to inter-variable correlations. These preliminary results suggest that painterly methods may provide an effective means for visualizing multi-dimensional quantities effectively.

2.6 Summary

The methods we employed produce images that are visually rich and represent many values at each spatial location. From different perspectives, they show the data at different levels of abstraction – more qualitatively at arm's length, more quantitatively up close. Finally, the images emphasize different data values to different degrees, leading a viewer through the temporal cognitive process of understanding the relationships among them.

We visualize quantities that have rarely been viewed before: rate of strain, turbulent charge, and turbulent current. We visualize these new quantities together with more commonly viewed quantities, allowing a scientist to use previously acquired intuition in interpreting the new values and their relationships to one another and to the more traditional quantities.

Our visualization of the rate of strain tensor combined with both the velocity and vorticity fields provides a unique pedagogical tool for explaining the dominant mechanisms responsible for certain fluid flow phenomena. Because an understanding of the deformation tensor (i.e. $\partial u_i/\partial x_j$) is of paramount importance for one's understanding of fluid flow phenomena, visualizing its symmetric and antisymmetric parts separately (i.e. the rate of strain tensor and the vorticity, respectively) clearly accentuates the interplay between rotational and shearing mechanisms within the flow.

The visualization of turbulent charge and turbulent current combined with both velocity and vorticity allows us to use knowledge concerning the latter fields in our effort to understand the usefulness of the newly visualized quantities. It is evident from the visualizations shown that, unlike vorticity, the turbulent charge and the turbulent current are far more localized. This validates the conjectures about the potential usefulness of the model, and also suggests that we focus our attention on viewing the turbulent charge and turbulent current

regions close to the surface of the cylinder. By focusing our examination to regions close to the cylinder, we see a high visual correlation between regions where turbulent charge accumulates and regions of vorticity generation.

By visualizing velocity with all the subsequently derived quantities presented here, we can observe through one visualization multiple properties of the flow. The freedom to display multi-valued data simultaneously allows us to get a more complete idea of both the dynamics and the kinematics of the flow, and hence provides a catalyst for future understanding of more complex fluid phenomena.

Chapter 3

DOGL - Distributed OpenGL using MPI

In our attempt to use an immersive environment for fluid flow visualization, our first obstacle was attempting to obtain software written for the expressed intent of visualization with our four-walled immersive environment driven by IBM hardware, a distributed memory-based system.

3.1 Motivation

Nearly all tiled display environments such as a Cave or PowerWall are driven by shared-memory graphics systems. However, distributed memory-based graphics systems that can produce comparable performance to typically more expensive shared-memory-based graphics systems are becoming more commonplace.

The key problem to substituting a distributed memory-based graphics system for a shared-memory graphics system is that, in general, there are no easy-to-use software libraries available for managing rendering clusters of graphics adapters. Worse, no commonly available library for driving tiled displays (e.g., Performer [32], CAVE library (tm) [33], VR Juggler [34], WorldToolKit [35]) support distributed rendering in a nearly transparent manner. Some libraries are also not available on all architectures.

We developed DOGL to begin to address the distributed rendering problem at our facility where we are driving our four-wall Cave with four or more graphics adapters in multiple nodes of our IBM SP running AIX. DOGL is an acronym for "Distributed OpenGL" and describes our approach to addressing the problem: all OpenGL calls from one process

are intercepted and are subsequently broadcast to multiple graphics adapters. DOGL also allows OpenGL calls to be explicitly sent to individual graphics adapters.

3.2 Related Work on Distributed Rendering

There are two primary categories of previous work: "the Scenegraph" approach and the "Broadcast OpenGL" approach.

Scenegraph Approach

The original CAVE library (tm) [33], which is now administered by Virtual Reality Software and Consulting (VRCO), ran in a distributed rendering environment through the use of a hardware-assisted shared-memory facility, Scramnet. This became largely obsolete when larger host systems capable of housing multiple graphics subsystems became available. Current VRCO developments includes implementations of CAVELib for Linux and HP systems, and will presumably include mechanisms for networked rendering distribution.

Java3D [36] may have the necessary components to solve the distributed tiled rendering problem, but it is not currently available for our target architecture. The performance of Java3D in a distributed environment may also be inadequate.

Before developing DOGL, we ran our Cave for about a year with "Jot", an in-house 3D interactive graphics system. Jot is capable of synchronizing scenegraphs between multiple Jot instances using a network connection. The primary problem with this approach is that the synchronization of the scenegraphs would frequently fail if synchronization code was not properly maintained by developers. The larger problem is that Jot was not originally designed to drive a Cave; it is a research system that evolves daily and, in particular, serves as a base-framework for several projects not related to the Cave. This problem combined with the absence of complete regression tests for simulating user interaction in the Cave enabled non-Cave project members to unknowingly cause Cave applications to fail. It was decided that both re-designing Jot and developing a new system to drive the Cave would be more costly than to design and develop DOGL. In fact, as expected, it only took a few weeks to get DOGL up and running for our needs.

Broadcast OpenGL Approach

Theoretically, GLX [37] could be used to drive a distributed tiled display. However, such a system would send OpenGL commands to multiple graphics sequentially rather than by

broadcasting them. There is also a nontrivial cost to frequently switching the OpenGL graphics context.

Humphreys et al. developed a system for driving large tiled displays [38] that functionally is a superset of DOGL. The primary differences between the two systems are: 1) DOGL is designed to support a single OpenGL application whereas Humphreys' system supports multiple, simultaneous window-based applications, and 2) DOGL uses MPI to broadcast efficiently data to rendering clients.

Humphreys et al.'s system evolved into WireGL [39] which is an example of a system that makes it very easy for the user and application programmer to leverage scalable rendering systems. Specifically, no modification to an OpenGL program is needed to run it on a tiled display. These and other systems work by intercepting normal (non-parallel) OpenGL calls and multicasting them, or channeling them to specific graphics processors. WireGL includes optimizations to minimize network traffic for a tiled display and, for most applications, provides scalable output resolution with minimal performance impact. The rendering subsystem relies not only on parallelism, but also on traditional techniques for geometry simplification such as view-dependent culling. To run a sequential OpenGL program written for a conventional 3D display device without modification requires that the "interceptor" deal with the complexities of managing head-tracking and stereo. In particular, this requires transformations that conflict with those in the original OpenGL code. Furthermore, any additional interaction devices must be provided by the application programmer.

The Scalable Display Wall [40] is driven by a network of PC's with 3D graphics accelerators. Normal OpenGL programs run on the display wall after copying a special DLL library into the same directory as the application. This system does not use MPI for networking and runs on only one architecture at this time.

3.3 Design

The primary design feature of DOGL is that it was to be minimally invasive; that is, programmers which had developed OpenGL code for desktop applications would be able to easily transition to running their application in the Cave with minimal code additions or changes. To accomplish this goal, DOGL is designed to intercept all OpenGL calls made by the master application and to distribute them to a collection of "rendering engines" (DOGL clients). From the programming perspective, only a few DOGL initialization calls for setting up the MPI environment and projection matrices for each wall of the Cave, along with linking with the DOGL library allow the programmer to quickly get their application

up and running in a Cave.

After initialization, each OpenGL call that the master program (called a DOGL server) makes is intercepted, and the necessary function arguments stored within a buffer. Immediately after buffering the call, the server then makes the OpenGL call and returns any necessary values to the calling application. DOGL also allows OpenGL calls to be explicitly sent to individual graphics adapters in the cluster. Once the buffer has attained a certain user set size (the size of which is currently determined by familiarity with the capabilities of the system on which one is running), the buffer is broadcast to the DOGL clients for rendering. A diagram of this is presented in Figure 3.1. Once a DOGL client has obtained a buffer of executable commands, it merely runs through its buffer executing each OpenGL command in the order in which they were placed in the buffer. Synchronization occurs when the frame buffers are swapped by calling synchronization calls within MPI.

The nomenclature used here is different from that of an X-Windowing system. Our assignment of the terms "server" and "client" to the functions of particular nodes came from our scientific computing experience. The term server here is used to refer to that node which is always initiating broadcast calls, and clients are those nodes which are always only receiving broadcast calls.

DOGL only enables a subset of OpenGL programs to run on a distributed memory-based graphics system. The restriction is that the state of and data from remote clients can not be queried. However, the state and data can be queried from the master node. Currently, DOGL's master node is used to run both the primary application and the renderer. This implies that OpenGL state is implicitly held by the OpenGL adapter which resides on the master node. Hence when OpenGL state information is necessary, OpenGL state calls can be used on the master node to obtain information which is indicative of the state on each client node. If the master node does not have a graphics adapter, but rather merely broadcasts all OpenGL information to rendering nodes, then it would be necessary either to maintain some of the OpenGL state information on the master, or to develop a communications strategy for retrieving information from remote nodes. For simplification, we chose to have the master node run both the application and to be one of the rendering nodes. For many applications this is not a problem.

3.4 MPI

The Message-Passing Interface (MPI) is one of the most widely used communication libraries used within scientific computing [41]. This standardized library runs on almost

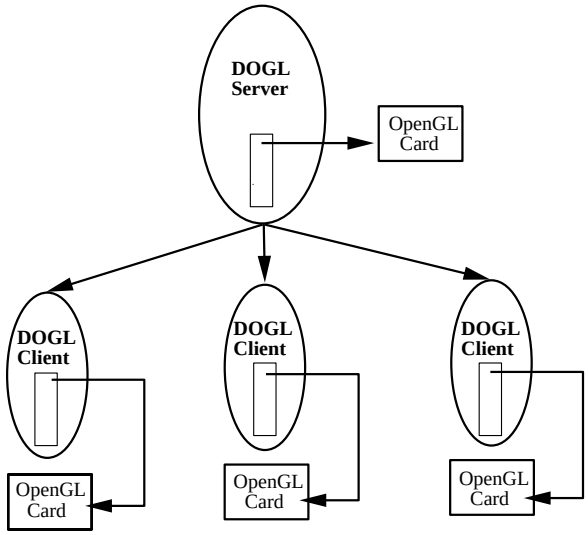

Figure 3.1: Diagram denoting the relationship between the DOGL server and clients.

every platform that can be used within the field of scientific computing, from networked PC clusters running under ethernet to IBM SPs communicating via a their proprietary high-speed switch. MPI is designed to work in the most general of parallel computing environments, the fully distributed environment. Although MPI at the implementation level may take advantage of the shared-memory capability of a particular hardware, the program remains focussed on the distributed memory model for parallel programming. We chose to use MPI for two major reasons: simplicity and portability.

3.4.1 Simplicity of DOGL-MPI Programming Model

Very few MPI calls are necessary in the current DOGL programming model. Other than the standard initialization calls which are necessary prior to invoking any message passing calls, the backbone of DOGL's communications is MPI_Bcast. The MPI_Bcast call broadcasts a buffer from one MPI process to all other MPI processes within the same MPI communications world. Each DOGL client calls MPI_Bcast to receive its buffer of OpenGL calls, and then proceeds to execute the commands contained within the buffer.

We chose to use MPI_Bcast for one primary reason: MPI_Bcast most closely accomplishes what DOGL requires, the distribution of all OpenGL calls from the master application (the DOGL server) to all DOGL clients. Although this could be accomplished by a loop which sends an identical buffer to each DOGL client, this methodology only admits optimizations for one-to-one communication. The beauty of MPI is that each hardware vendor can optimize MPI for their particular hardware configuration without changing the

API. Hence, in the case of MPI_Bcast, a vendor may choose to implement this command by looping over all MPI processes and sending one-to-one communications; however, the vendor is allowed the freedom to optimize the broadcast to utilize hardware features such as hardware multicast. In addition, since MPI is commonly used within the scientific computing community, optimization of MPI on a variety of platforms is certain as vendors attempt to set their mark within the area of high performance computing. Since these optimizations are at no cost to the application programmer, MPI allows the user to develop code which will continue to improve as computing hardware and MPI software developments progress.

3.4.2 Portability of DOGL-MPI Programming Model

MPI allows the programmer to develop parallel code with no knowledge of the underlying hardware. This is particularly advantageous to those people who do not wish to be tied down to a particular hardware vendor. Although most people have a vendor of choice, quite often a computer graphics lab consists of a plethora of different machine types. Again, due to MPI's prevalence in the scientific computing world, MPI runs on a wide variety of platforms with no modification to the code. From commodity PCs running under Linux or WinNT, to supercomputers such as IBM SPs and Origin 2000s, MPI allows for an easy software transition of DOGL to any platform which supports both MPI and OpenGL.

3.5 Implementation

An example DOGL function is presented in code form below. In the master application, a call to glVertex3d would be intercepted, and instead doglVertex3d would be called. The variables dogl_command and dogl_psize are used in the packing of the buffer. The first variable, dogl_command, denotes which OpenGL command was called. The second variable, dogl_psize, denotes the size in bytes needed to pack this command into the buffer. The arguments are first copied into temporary storage, and then an if-statement is executed to determine whether DOGL server or DOGL client commands should be executed.

If the DOGL server (the master application) has called this function by the interception of an OpenGL call, then first the buffer is checked to make sure that sufficient space is available to store all data necessary for the OpenGL command. If there is not sufficient space on the buffer, then the buffer is broadcast to the clients (thus emptying the buffer). After verification of buffer space is guaranteed, then both the command and the necessary arguments are packed into the DOGL buffer. Finally, the DOGL server executes the OpenGL call and the function returns.

```
void doglVertex3d (GLdouble x, GLdouble y, GLdouble z){
  int dogl_command = DOGL_GLVERTEX3D;
  int dogl_psize = sizeof(int) + 3*sizeof(GLdouble);

  GLdouble aval[3];

  aval[0] = x;
  aval[1] = y;
  aval[2] = z;

  if(mynode == mpiroot){
    doglPrepareBuffer(dogl_psize);
    doglPackBuffer(&dogl_command, sizeof(int));
    doglPackBuffer(aval ,3*sizeof(GLdouble));
  }
  else{
    doglUnpackBuffer(aval,3*sizeof(GLdouble));
  }

  glVertex3d(aval[0],aval[1],aval[2]);

  return;
}
```

The DOGL client, upon receipt of a buffer, extracts the OpenGL function calling info packed by the server. This information is used to determine which DOGL command is to be executed on the client. In this case, the client would extract the dogl_command from the buffer, from which it would know to call doglVertex3d. When doglVertex3d is called on the client, the second part of the if-statement is executed, and hence the three doubles used as arguments in the original function call are then unpacked into the temporary storage space. The OpenGL command glVertex3d is then called on the client, and the function returns.

3.6 Utilization

This section goes over information needed to use DOGL. Specifically, code modifications, overriding the default broadcast behavior of commands, and how to run a DOGL program.

3.6.1 Code modifications

An OpenGL application must be modified to work with DOGL. First, the main function needs to be changed such that DOGL calls are made before and after the original application starts. To illustrate, the following code is a template for a generic OpenGL application:

```
void main( int argc, char **argv )
{
   // Begin OpenGL application
   run_app();
}
```

The necessary modifications are:

```
void main( int argc, char **argv )
{
   // 1. handle DOGL & MPI initialization
   doglInit();

   // 2. Set the DISPLAY environment variable.  The display
   // name used can be determined by a configuration file.
   char cmd[256];
   sprintf(cmd, "DISPLAY=%s", get_display_name(doglGetID()));
   putenv(cmd);

   // 3. Start the main application
   if (doglGetID() == 0) {
      // if running as master, begin OpenGL application...
      run_app();
   } else {
      // ...otherwise run as a "DOGL client", a procedure
      // that is part of DOGL and handles rendering on
```

```
      // non-master display adapters.
      dogl_client();
   }

   // 4. clean up
   doglFinalize();
}
```

3.6.2 Overriding Broadcast Behavior

By default, DOGL broadcasts all OpenGL calls made by the master application to all the clients. This is undesirable in some situations. For example, in the Cave each wall normally has a unique projection matrix.

To support this in DOGL, each OpenGL command has an new call with one additional integer parameter. The name of the new call has a "do" prefix (e.g., "glLoadMatrixd" becomes "doglLoadMatrixd"). This new call behaves exactly the same as the old one, but is only executed on the node with ID equal to the integer value passed in.

For example, in the case of the Cave this pseudo-code is used:

```
void load_projection_matrices()
{
   // for each wall of the Cave, load a unique matrix
   for(int i=0;i<num_walls;i++) {
      GLdouble mat[16];

      // compute a projection matrix based on the
      // specific screen description and head tracking
      // data given and assign it to 'mat'.
      compute_projection_matrices(screen_desc[i],
                                  head_desc,
                                  &mat);

      // send matrix 'mat' to i-th node.
      doglLoadMatrixd(mat, i);
   }
}
```

3.6.3 Running a DOGL program

DOGL converts a conventional executable into a "MPI" executable. Each architecture may have a slightly different procedure for executing an MPI executable. However, To give a sense of what's involved, the following code is sufficient to execute a DOGL program on an IBM:

```
setenv MP_EUILIB ip
setenv MP_EUIDEVICE css0
setenv MP_PROCS 4
setenv MP_HOSTFILE host_config_file
/usr/bin/poe dogl_executable
```

In the example above, "MP_PROCS" is set to 4, so the "MP_HOSTFILE" environment variable must point to the ASCII file containing the four node names on which DOGL is to run.

3.7 Results

The primary result of this work was a working system that we are using with a distributed rendering environment to drive our four-wall Cave. Specifically, we have used DOGL to develop a prototype system for visualization blood flow through an artery described in the next chapter and several students used it for on-going projects and course work including an initial implementation of the "Cave Painting" program.

We accomplished some preliminary measurements of DOGL's performance. All performance measurements discussed herein were accomplished on the IBM SP gnodes a and b at the Center for Advanced Scientific Computation and Visualization at Brown University. The only adjustable parameter within the DOGL system is the packet size used for transmission of the buffered OpenGL calls. Figure 3.3 plots the performance of DOGL measured in frames per second verses the packet size used for various triangle counts. Observe that there exists a minimum packet size, around two kilobytes, which should be used for maximum performance. This packet size indicates the tradeoff point between network latency and bandwidth on the IBM SP. In Figure 3.3 we plot the the performance of DOGL measured in frames per second verses the number of triangles for various packet sizes. This plot demonstrates the effect of increased triangle counts on the total time, which consists of both the networking and rendering time on the IBM hardware available.

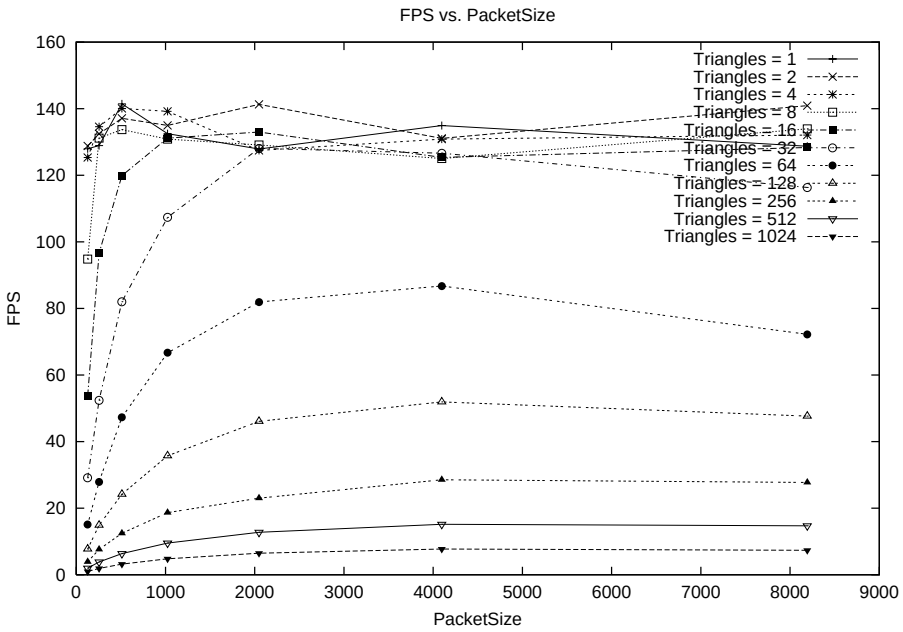

Figure 3.2: Frames per second verses packet size for various triangle numbers using the IBM switch in userspace mode.

In the blood flow visualization system, the frame rate is between 20 and 30 frames per second (FPS). This rate can drop to between 5 and 20 FPS when several visualization techniques are displayed. However, this drop in frame rate is definitely influenced by non-graphics computations, such as moving particles through the flow, that are running on the same processor as the geometry processing for our current OpenGL implementation. Moving graphics and visualization tasks to different processors is an important next step to improve performance.

While we primarily run DOGL on our IBM system, we have also run it on our SGI system.

As reported in [38], using display lists greatly reduces network traffic. This implies that a scene consisting of dynamic geometry that changes from frame to frame is a worst-case scenario for DOGL. We have not yet been restricted by this scenario, however, we also have not written contrived applications that avoid it. Future work will analyze the overall performance of DOGL including both static and dynamic geometry, but the high-level performance result is DOGL is capable of driving a Cave at interactive rates.

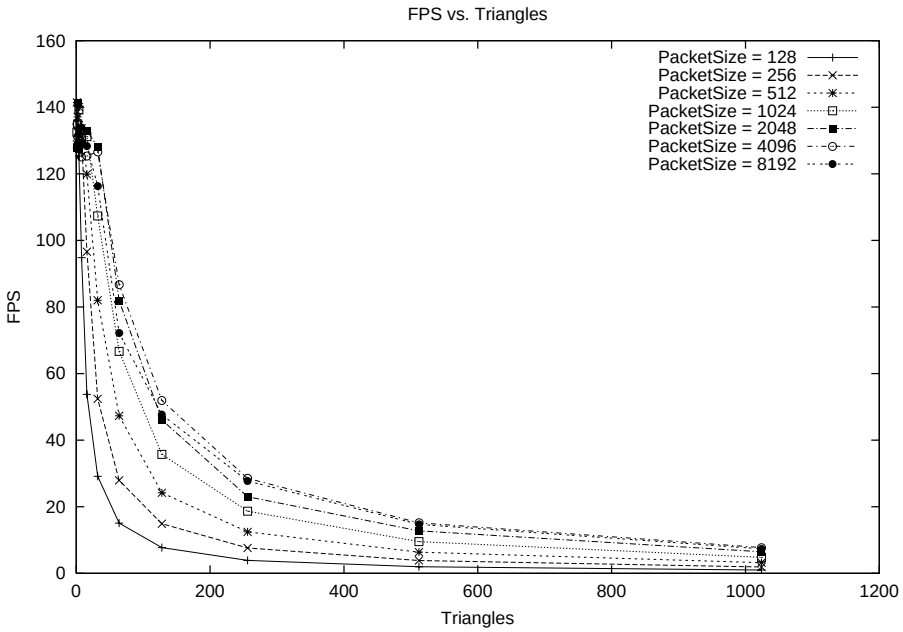

Figure 3.3: Frames per second verses triangle count for various packet sizes using the IBM switch in userspace mode.

Chapter 4

Arterial Flow in a Bypass Graft: A Case Study

Given the computational and graphical hardware capabilities present here at Brown, we desired to combine simulation and visualization into a package which would utilize the interactive, immersive environment housed at Brown's Center for Advanced Scientific Computation and Visualization. As a first stage in this effort, we chose to combine two research codes developed at Brown: $\mathcal{N}\varepsilon\kappa\mathcal{T}\alpha r$, a computational fluid dynamics code developed under the direction of Professor George Karniadakis in the Division of Applied Mathematics, and "Jot", a graphical user interface research code developed under the direction of Professor Andries van Dam in the Department of Computer Science. Specifically, as a first step, we developed a software interface which allowed Jot to load and manipulate $\mathcal{N}\varepsilon\kappa\mathcal{T}\alpha r$ geometry and flow data files. This first step allowed us to take three dimensional simulations of fluid flow phenomena created by $\mathcal{N}\varepsilon\kappa\mathcal{T}\alpha r$, load them into Jot, and to use software tools engineered into Jot for the interaction with, and manipulation of, the flow data.

4.1 Immersive Environments for Scientific Visualization

The use of virtual environments for visualizing fluid flow phenomena is not new. The Virtual Windtunnel [42] visualizes air flow around geometric objects such as the space shuttle. Our system differs in terms of the actual application– blood flow versus air flow visualization.

The combination of the Virtual Director[43] VR interface and the CAVE5D[44] visualization system is one of the few virtual reality-based scientific visualization applications that uses multimodal input. However, their system combines voice and wand input which limits

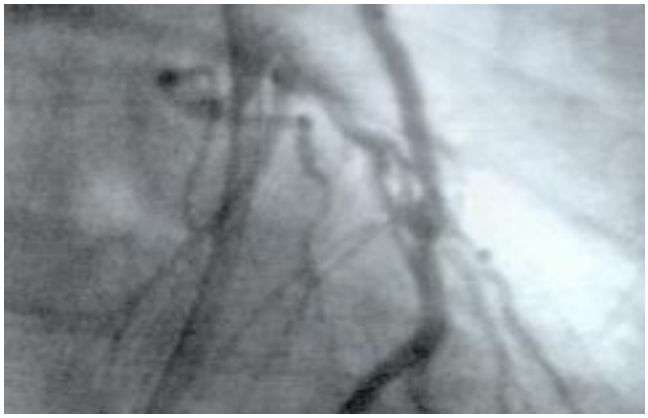

Figure 4.1: One image from an angiogram showing the "bird's eye" view that doctors are typically limited to. These angiograms give an excellent image of where problems lie, but are not very reliable indicators of the genesis of lesions.

the naturalness of their interface since users will typically only interact with one hand. By combining voice and whole-hand input using Pinch Gloves instead of a wand, our system allows users to interact with two hands which has been shown to be beneficial for many interaction tasks[45].

4.2 Problem Statement

In a multi-disciplinary effort, we used our newly designed system in an attempt to understand the haemodynamic effects due to three-dimensional modifications of the geometry within arterial bypass grafts. Atherosclerotic lesions tend to develop near areas of flow disturbances such as at arterial branches and bifurcations.

Fig. 4.1 shows one image from an angiogram of a damaged artery. Images like these are current state-of-the-art for how clinicians view blocked arteries. Angiograms are effective for showing the degree of blockage in an artery but do not show why or how future lesions may form.

Although a great deal of flow data has been obtained experimentally, certain flow quantities which are inaccessible to the physician using commonly available clinical techniques can be modeled accurately through the use of numerical simulation. Fig. 4.2 shows output from tecplot [46], a widespread fluid dynamics visualization package. We believe that an immersive environment can permit more effective visualization of fluid simulation results than conventional desktop display devices. tightly-coupled interdisciplinary project is aimed at understanding how to reduce the failure rate of these grafts. To this end, we designed and

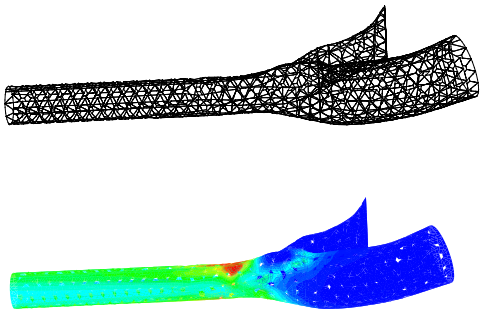

Figure 4.2: Image created in tecplot showing a typical visualization that might be used to explore simulated flow data within an artery. The top image shows the geometry in wireframe while the bottom image shows wall shear stress magnitude mapped to the vessel surface. Exploration using tools like tecplot are less interactive than the immersive visualization environment we describe.

implemented an immersive system for exploring numerically simulated flow data through a model of a coronary artery graft. Key software components were obtained from $\mathcal{NEKTAR}$ and from Jot. $\mathcal{NEKTAR}$-Jot, combined with DOGL, allowed us a mechanism for exploring the multi-valued data simultaneously for the purpose of exploring potential sources of future lesions. We present an example session using the system and discuss our experiences developing, testing, and using it.

4.3 Simulating Complex-Geometry Flows with $\mathcal{NEKTAR}$

The flow solver corresponds to a particular version of the code $\mathcal{NEKTAR}$, which is a general purpose CFD code for simulating incompressible, compressible and plasma flows in unsteady three-dimensional geometries. The major algorithmic developments are described in [47] and [1]. The code uses meshes similar to standard finite element and finite volume meshes, consisting of structured or unstructured grids or a combination of both. The formulation is also similar to those methods, corresponding to Galerkin and discontinuous Galerkin projections for the incompressible and compressible Navier-Stokes equations, respectively.

4.4 Simulation/Visualization Coupling

Maintaining a common data format for the numerical simulation software and for the visualization software helped us to iterate more quickly and experiment with more interaction and rendering techniques. In an early prototype of our system the simulation data had to be reformatted significantly before the visualization system could process it. We found that significant time was spent doing this reformatting. In our second visualization system, we built a library to access the simulation data directly. Although the library took some time to implement, the increased coupling between simulation and visualization more than paid off with faster iterations and less wasted time on data conversions. It also helped keep the thrust of the work at a higher level where we could concentrate more on the science and less on the data.

The library which we developed contained interfacing code between $\mathcal{N}\varepsilon\kappa\mathcal{T}\alpha r$ and Jot. This software layer consisted of a NEKTAR_DATA class constructed into the Jot class hierarchy. This class contains methods for loading and manipulating $\mathcal{N}\varepsilon\kappa\mathcal{T}\alpha r$ geometry and simulation data. The following functionality has been created:

- Load reference geometry.
- Load fluid flow simulation data (velocity and pressure).
- Compute important derived quantities (vorticity, divergence and wall shear stress).
- Generate streamlines.
- Generate isosurface information (for use with NOISE, University of Utah's interactive isosurfacing system [48]).
- Allow the sampling of data at an arbitrary point in the domain.

The above functionality was created with the specific purpose of successfully creating an arterial bypass graft demonstration. However, the functionality provided is not specific to arterial flows, and hence this interface provides a general means of interacting with $\mathcal{N}\varepsilon\kappa\mathcal{T}\alpha r$ generated fluid flow data.

4.5 A Virtual Cardiovascular Laboratory

An example user scenario in the virtual cardiovascular laboratory describes its functionality. A few frames illustrate the main points.

Figure 4.3: A view of the immersive artery visualization looking at the bifurcation where the graft enters the original artery. The visualization is within a 4-wall cave, with head-tracked stereo. A gestural interface provide easily-learned interaction techniques for navigating through the environment and for studying the flow.

The session begins with an overall view of the bifurcated artery, which shows both the originally blocked artery, and the newly grafted segment into which the blood now flows.

Since the vascular geometry is the primary determinant of the flow field, the researcher begins by examining the reference geometry. Here, the reference geometry is manipulated using a combination of hand gestures. A 3D tracker locates each hand and pinch gloves [49] provide information about relationships between fingers. The user places himself at the entrance of the bypass graft by gesturally pulling himself through space and begins to examine the artery structure and moves further down the artery to investigate the area of the bifurcation, shown in Fig. 4.3.

The user selects tools from a virtual tool-belt around his waist and controls these tools using both voice commands and hand gestures. Tools can be retrieved from the tool-belt when the user looks down, as he is demonstrating in Fig. 4.4. To orient himself to the flow conditions, the researcher uses two different particle advection widgets. The first, a dust widget, allows the user to throw particles into the flow just as if he were throwing chaff into the wind. This type of normal action allows the user to comfortably acclimate himself to the flow conditions. Although convenient, this widget is not very precise. For a more precise and persistent stream of particles, the metaphor of a fizzing "alkaseltzer tablet" is used. Using this widget, the researcher interactively places particles precisely in areas of interest and watches as the particles are advected along by the natural flow of blood. This type of interactive investigation gives the researcher an initial indication of the flow patterns

Figure 4.4: When the user looks down a toolbelt appears. Tools include dust, for advecting particles through the flow; a widget for choosing wall coloring; a round alkaseltzer widget for creating a persistent source of advecting particles; an isosurface "microphone" widget (the square cube here); and a streamline and rake widget.

within this complex system.

Leaving the alkaseltzer tablet in place, the user places an interactive rake widget in the region of the advecting fluid particles. Here, streamlines at one instant of time are examined. Streamlines are lines which run tangential to the velocity at any given point. Hence streamlines give to the researcher an idea of the currents of blood flow through which the particles are traveling.

The researcher switches to a single streamline widget for investigating a particular region of interest. The streamline dips near the bifurcation, indicating a flow disturbance. The researcher then uses the streamline as guide, just like a rope, as he traverses down the bypass past the graft and into the original artery.

Rotating himself 180 degrees with two-handed interaction, the researcher sees the blockage that the bypass is intended to alleviate.

Low flow velocity can lead to regions with long particle "residence times". Regions like these are correlated with thrombus formation and to possible plaque formation which can lead to graft failure. To investigate regions of slow flow, three widgets are used. First, the researcher uses a reverse streamline widget to examine the region of the blockage. The fact that this streamline at first bends significantly, and then ends abruptly as the user moves it into the blocked region demonstrates what the researcher suspected, that the fluid between the blockage and the graft entrance is stagnant.

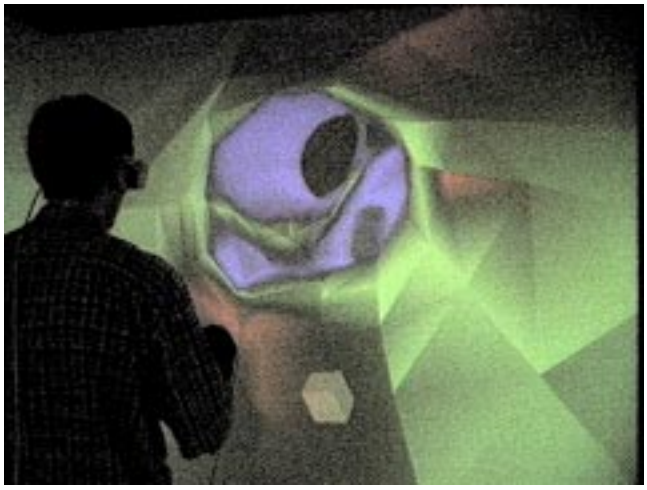

Figure 4.5: Wall shear stress is encoded in wall color, with blue showing low values, green midrange values, and red high values. Regions of low shear stress tend to be correlated with sites of future lesions.

The researcher then uses the alkaseltzer widget to place particles around the stagnation area. What becomes immediate apparent is the relative stagnation of the particles placed within the blocked artery as opposed to the particles flowing through the newly grafted artery.

A gray cube isosurface microphone widget creates isosurfaces which help expose the gross features within the flow region. Low order isosurfaces increase interactivity; high order isosurfaces are available to show greater flow detail. Isosurfaces are computed at interactive rates by the NOISE isosurface extraction system developed at the University of Utah's Center for Scientific Computing and Imaging [48].

The researcher then examine wall shear stress mapped to the color of the vessel walls, a quantity which was previously unavailable using either clinical or experimental techniques (see Fig. 4.5). Quantities like wall shear stress can give important insights into flow behavior [50, 51, 52, 53]. Since the bypass graft is much larger than the original diseased artery, the flow velocity within the bypass graft is slower than that of the flow downstream of the bypass in the smaller diameter artery. This naturally implies a lower relative shear stress in the bypass compared to the original diseased artery. Also of interest to the researcher are anomalous regions of shear stress. The researcher notices a region of extremely high mean shear stress immediately downstream of the bypass entry point. Just as if you were pointing a garden hose of running water at the floor, we see a region downstream of the graft in which the shear stress is much higher than what the original unblocked artery had

experienced. The examination of these types of anomalies within the bypass flow system are regions of interest to both flow researchers and physicians.

Chapter 5

Summary and Conclusions

We chose to investigate two particular CFD visualization techniques: using concepts from painting for visualizing multi-valued data for two dimensional flows, and using immersive environments for visualizing fluid flow data for three dimensional flows. For our two dimensional visualizations, our objective was to provide the *seamless* integration of multiple flow quantities into one visualization. For our three dimensional visualizations, our objective was to utilize our interactive, immersive environment here at Brown for fluid flow visualizations of simulation data produced by the computational fluid dynamics code $\mathcal{NEKTAR}$. Our projects had the following milestones:

- The painterly methods we employed produced images that are visually rich and represent many values at each spatial location. From preliminary user-study data obtained in a pilot user-study, we concluded that these methods allow the viewer to identify more rapidly and more accurately the correlation between different flow quantities. Our hope is that in addition to accelerating the process of identifying correlations, the viewer will be able to use this method to postulate new correlations between flow quantities which have not yet been identified.

- We visualized quantities that have rarely been viewed before: rate of strain, turbulent charge, and turbulent current. Doing so provided us with a good testbed for attempting to understand how scientists visually correlate quantities.

- We developed DOGL, a distributed OpenGL software library which broadcasts via MPI OpenGL commands to multiple graphics adapters.

- We developed a software interface useful for visualization applications (such as Jot) for the CFD code $\mathcal{NEKTAR}$. The interface was an approximately 2000 line C++ class

which encapsulated the internal data format of $\mathcal{NEKTAR}$. Methods for evaluating field values at an arbitrary point within the computation domain, for calculating streamlines given a collection of starting points, and for computing derived quantities such as vorticity and wall shear-stress were implemented. The high-level goal for the development of this interface was to provide a bridge between the software of the graphics group in Computer Science and Professor George Karniadakis' group (the CRUNCH group) in Applied Mathematics.

- We successfully demonstrated the merger of $\mathcal{NEKTAR}$, Jot, and DOGL in the examination of the simulation of an arterial bypass graft.

Due to the highly collaborative nature of the projects presented in this project report, it is necessary to comment on the components of this work which are significantly mine from those accomplished by others involved in these projects. My primary role in all of the projects presented in this report was as a mediator between the graphics group and the CRUNCH group. As a Ph.D. student in Applied Mathematics and a Sc.M. student in Computer Science, I had the unique opportunity of helping instigate collaborative efforts between the two groups. My primary contribution to all the work presented herein was as a consultant; I actively strived to incorporate both solid mathematical and fluid science concepts into the collaborative effort. In addition to my role as consultant, I programmed both DOGL and the $\mathcal{NEKTAR}$ interface.

The projects presented herein benefited greatly from the work of many others. For the two dimensional painterly concepts, modules written in AVS by Professor David Laidlaw were used, and final renderings of the visualizations were produced by Professor Laidlaw for our Visualization '99 paper [26] . Interpretations of the visualization of turbulent current and turbulent charge were accomplished by Dr. Haralambos Marmanis, the co-author with me of the Visualization '99 paper [26].

For both DOGL and the artery work, I benefited greatly from Andrew Forsberg's help with interfacing both codes with Jot. All Jot-specific work was accomplished by Andrew Forsberg.

5.1 Lessons Learned

Multi-valued data presentation using painterly methods shows tremendous promise. Many scientific endeavors require the simultaneous viewing of multiple pieces of data in order to understand a particular phenomena. The two dimensional visualizations presented here

demonstrate the potential of this methodology. Future work includes the comparison of these painterly methods with commonly used plotting techniques for visualizing two dimensional fluid flow data, and extending the painterly rendering techniques to three dimensional fluid flow data.

DOGL was born out of necessity; no consistent, reliable software was available to us at the time to visualize fluid flow data in the Cave. Quite often the effort invested in getting a particular demonstration ready for a deadline would lead to weeks of re-engineering, with no forethought for the next possible demonstration. We thus decided to develop DOGL to allow us to run Jot consistently in the Cave. This allowed Jot to continue along its normal, desktop-environment development cycle, with minimum intrusion for distributed rendering needs. After having almost finished the implementation of DOGL we learned about WireGL [39]. Much effort has been put into optimizing WireGL, and hence after completing the arterial bypass graft case study we decided not to persue DOGL, but rather to focus on understanding WireGL, and seeing how we might integrate it into our existing software infrastructure.

We also have presented a virtual environment for visualization of fluid flow through a simulated arterial graft. This environment allowed both visualization and interaction with the output of the CFD code $\mathcal{NEKTAR}$. The effort of combining $\mathcal{NEKTAR}$ with Jot illuminated many of the problems associated with interacting with large data. Issues such as effective use of concurrent processing and efficient data management stood out as the next step for consideration in the evolution of this project.

Use of the environment shows good potential for helping to develop our understanding of failure modalities for these grafts and, hopefully, for reducing their failure rate. Doctors speculated that they would potentially be able to combine the currently available clinical knowledge with information that could be discovered in the Cave to pose new hypotheses about lesion genesis and progression.

Bibliography

[1] T.C.E. Warburton. *Spectral/hp Methods on Polymorphic Multi-Domains: Algorithms and Applications*. PhD thesis, Division of Applied Mathematics, Brown University, 1999.

[2] P.G. Saffman. *Vortex Dynamics*. Cambridge University Press, Cambridge, UK, 1992.

[3] C. Evangelinos. *Parallel Simulations of Flexible Cylinders subject to VIV*. PhD thesis, Division of Applied Mathematics, Brown University, 1999.

[4] David H. Laidlaw, Eric T. Ahrens, David Kremers, Matthew J. Avalos, Carol Readhead, and Russell E. Jacobs. Visualizing diffusion tensor images of the mouse spinal cord. In *Proceedings Visualization '98*. IEEE Computer Society Press, 1998.

[5] Lambertus Hesselink, Frits H. Post, and Jarke J. van Wijk. Research issues in vector and tensor field visualization. *IEEE Computer Graphics and Applications*, 14(2):76–79, 1994.

[6] K Jain. *Fundamentals of Digital Image Processing*. Prentice Hall, 1989.

[7] Joe P. Windham, Mahmoud A. Abd-Allah, David A. Reimann, Jerry W. Froelich, and Allan M. Haggar. Eigenimage filtering in MR imaging. *Journal of Computer-Assisted Tomography*, 12(1):1–9, 1988.

[8] Robert B. Haber and David A. McNabb. Visualization idioms: A conceptual model for scientific visualization systems. *Visualization in scientific computing*, pages 74–93, 1990.

[9] Herman Chernoff. The use of faces to represent points in k-dimensional space graphically. *Journal of the American Statistical Association*, 68(342):361–368, 1973.

[10] Robert F. Erbacher, Georges Grinstein, John Peter Lee, Haim Levkowitz, Lisa Masterman, Ron Pickett, and Stuart Smith. Exploratory visualization research at the University of Massachusetts at Lowell. *Computers and Graphics*, 19(1):131–139, 1995.

[11] Victoria Interrante, Henry Fuchs, and Stephen M. Pizer. Conveying the 3D shape of smoothly curving transparent surfaces via texture. *IEEE Transactions on Visualization and Computer Graphics*, 3(2), April–June 1997. ISSN 1077-2626.

[12] Victoria L. Interrante. Illustrating surface shape in volume data via principal direction-driven 3D line integral convolution. In Turner Whitted, editor, *SIGGRAPH 97 Conference Proceedings*, Annual Conference Series, pages 109–116. ACM SIGGRAPH, Addison Wesley, August 1997. ISBN 0-89791-896-7.

[13] Nelson Max, Roger Crawfis, and Dean Williams. Visualization for climate modeling. *IEEE Computer Graphics and Applications*, 13(4):34–40, July 1993.

[14] Roger Crawfis, Nelson Max, and Barry Becker. Vector field visualization. *IEEE Computer Graphics and Applications*, 14(5):50–56, 1994.

[15] Jarke J. van Wijk. Flow visualization with surface particles. *IEEE Computer Graphics and Applications*, 13(4):18–24, July 1993.

[16] Jarke J. van Wijk, Andreaj S. Hin, Willem C. de Deeuw, and Frits H. Post. Three ways to show 3d fluid flow. *IEEE Computer Graphics and Applications*, 14(5):33–39, 1994.

[17] Jarke J. van Wijk. Spot noise-texture synthesis for data visualization. In Thomas W. Sederberg, editor, *Computer Graphics (SIGGRAPH '91 Proceedings)*, volume 25, pages 309–318, July 1991.

[18] Brian Cabral and Leith (Casey) Leedom. Imaging vector fields using line integral convolution. In James T. Kajiya, editor, *Computer Graphics (SIGGRAPH '93 Proceedings)*, volume 27, pages 263–272, August 1993.

[19] Greg Turk and David Banks. Image-guided streamline placement. In Holly Rushmeier, editor, *SIGGRAPH 96 Conference Proceedings*, Annual Conference Series, pages 453–460. ACM SIGGRAPH, Addison Wesley, August 1996. held in New Orleans, Louisiana, 04-09 August 1996.

[20] Paul E. Haeberli. Paint by numbers: Abstract image representations. In Forest Baskett, editor, *Computer Graphics (SIGGRAPH '90 Proceedings)*, volume 24, pages 207–214, August 1990.

[21] Barbara J. Meier. Painterly rendering for animation. In Holly Rushmeier, editor, *SIGGRAPH 96 Conference Proceedings*, Annual Conference Series, pages 477–484. ACM SIGGRAPH, Addison Wesley, August 1996. held in New Orleans, Louisiana, 04-09 August 1996.

[22] Georges Winkenbach and David H. Salesin. Rendering parametric surfaces in pen and ink. In Holly Rushmeier, editor, *SIGGRAPH 96 Conference Proceedings*, Annual Conference Series, pages 469–476. ACM SIGGRAPH, Addison Wesley, August 1996. held in New Orleans, Louisiana, 04-09 August 1996.

[23] Georges Winkenbach and David H. Salesin. Computer–generated pen–and–ink illustration. In Andrew Glassner, editor, *Proceedings of SIGGRAPH '94 (Orlando, Florida, July 24–29, 1994)*, Computer Graphics Proceedings, Annual Conference Series, pages 91–100. ACM SIGGRAPH, ACM Press, July 1994. ISBN 0-89791-667-0.

[24] Michael P. Salisbury, Sean E. Anderson, Ronen Barzel, and David H. Salesin. Interactive pen–and–ink illustration. In Andrew Glassner, editor, *Proceedings of SIGGRAPH '94 (Orlando, Florida, July 24–29, 1994)*, Computer Graphics Proceedings, Annual Conference Series, pages 101–108. ACM SIGGRAPH, ACM Press, July 1994. ISBN 0-89791-667-0.

[25] Michael P. Salisbury, Michael T. Wong, John F. Hughes, and David H. Salesin. Orientable textures for image-based pen-and-ink illustration. In Turner Whitted, editor, *SIGGRAPH 97 Conference Proceedings*, Annual Conference Series, pages 401–406. ACM SIGGRAPH, Addison Wesley, August 1997. ISBN 0-89791-896-7.

[26] R.M. Kirby, H. Marmanis, and D.H. Laidlaw. Visualizing multivalued data from 2d incompressible flows using concepts from painting. In *Proceedings Visualization '99*. IEEE Computer Society Press, 1999.

[27] Philip A. Thompson. *Compressible-Fluid Mechanics*. Advanced engineering series. Maple Press Co., 1984.

[28] Rutherford Aris. *Vectors, Tensors, and the Basic Equations of Fluid Mechanics*. Dover Publications, Inc, New York, 1989.

[29] M.J. Lighthill. *Laminar Boundary Layers.* (ed. E. Rosenhead), Dover Publications, Inc, New York, 1988.

[30] H. Marmanis, Y. Du, and G.E. Karniadakis. Turbulent control via geometry modifications and electromagnetic fields. 1998.

[31] H. Marmanis. Analogy between the navier-stokes and maxwell's equations: Application to turbulence. *Phys. Fluids*, 10(6):1428–1437, 1998.

[32] J. Rohlf and J. Helman. Iris performer: A high performance multiprocessing toolkit for real-time 3d graphics. In *Proceedings of SIGGRAPH 94*, 1994.

[33] See http://www.vrco.com.

[34] See http://www.vrjuggler.org.

[35] See http://www.sense8.com.

[36] See http://java.sun.com/products/java-media/3d/index.html.

[37] See http://www.opengl.org/documentation/glx.html.

[38] G. Humphreys and P. Hanrahan. A distributed graphics system for large tiled displays. In *Proceedings Visualization '99*. IEEE Computer Society Press, 1999.

[39] Greg Humphreys, Ian Buck, Matthew Eldridge, and Pat Hanrahan. Distributed rendering for scalable displays. In *Proceedings IEEE Supercomputing 2000*. IEEE Computer Society Press, 2000.

[40] See http://www.cs.princeton.edu/omnimedia/index.html.

[41] P. Pacheco. *Parallel Programming with MPI.* Morgan Kaufmann, 1997.

[42] Steve Bryson and Creon Levit. The virtual windtunnel: An environment for the exploration of three-dimensional unsteady flows. In *vis 91*, pages 17–24, 1991.

[43] See http://virdir.ncsa.uiuc.edu/virdir.

[44] See http://www.ccpo.odu.edu/ cave5d/homepage.html.

[45] W. Buxton and B. Myers. A study in two-handed input. In *In* Proceedings of CHI '86, pages 321–326, 1986.

[46] See http://www.amtec.com. Amtec Engineering, Inc., Bellevue, WA 98005.

[47] S. J. Sherwin. *Triangular and Tetrahedral spectral/hp finite element methods for fluid dynamics*. PhD thesis, Princeton University, 1995.

[48] Y. Livnat, H.W. Shen, and C.R. Johnson. A near optimal isosurface extraction algorithm using the span space. *IEEE Transactions on Visual Computing*, 2(1):73–84, 1996.

[49] See http://www.fakespace.com.

[50] R.M. Nerem. Vascular fluid mechanics, the arterial wall, and atherosclerosis. *Journal of Biomechanical Engineering*, 114:274–282, 1992.

[51] J.E. Moore, D.N. Ku, C.K. Zarins, , and S. Glagov. Pulsatile flow visualization in the abdominal aorta under diering physiology conditions: implications for increased susceptibility to atherosclerosis. *Journal of Biomechanical Engineering*, 114:391–197, 1992.

[52] D.N. Ku and D.P. Giddens. Pulsatile flow in a model carotid bifurcation. *Arteriosclerosis*, 3:31–39, 1983.

[53] C.K. Zarins, D.P. Giddens, B.K. Bharadvaj, R.F. Mabon, , and S. Glagov. Carotid bifurcation atherosclerosis: quantitative correlation of plaque localization with flow velocity profiles and wall shear stress. *Circulation Research*, 53:502–514, 1983.